

Ideal Glass and Ideal Disk Packing in Two Dimensions

Viola M. Bolton-Lum¹, R. Cameron Dennis^{2,3}, Peter K. Morse^{4,5}, and Eric I. Corwin¹

¹*Department of Physics and Materials Science Institute, University of Oregon, Eugene, Oregon 97403, USA*

²*Department of Physics and Astronomy, University of Pennsylvania, 209 South 33rd Street, Philadelphia, Pennsylvania 19104, USA*

³*Department of Physics and Soft Matter Program, Syracuse University, Syracuse, New York 13244, USA*

⁴*Department of Physics, Seton Hall University, South Orange, New Jersey 07079, USA*

⁵*Department of Chemistry, Department of Physics and Princeton Institute of Materials, Princeton University, Princeton, New Jersey 08544, USA*



(Received 2 May 2025; revised 27 September 2025; accepted 8 December 2025; published 2 February 2026)

The ideal glass, a disordered system of particles with zero configurational entropy, cannot be realized through thermal processes. Nevertheless, we present a method for constructing ideal jammed packings of soft spheres, and thus the zero temperature ideal glass, in two dimensions. In line with the predicted properties, these critically jammed packings have high bulk and shear moduli as well as an anomalously high density. While the absence of pressure scaling in the shear moduli of crystalline materials is often attributed to the ordered nature of the particles, we show for the first time that disordered ideal packings also have this feature. We also find that the density of states avoids the low frequency power law scaling famously found in most amorphous materials, these configurations display hyperuniformity, and they melt at unusually high temperatures compared to conventional packings. In addition to resolving a long-standing mystery, this methodology represents a valuable shortcut in the generation of well-equilibrated glassy systems. The creation of such an ideal packing makes possible a complete exploration and explanation of two-dimensional jammed and glassy systems.

DOI: 10.1103/vldy-r77w

Introduction—A defect free crystal is the apex of order [1]. By contrast, when a liquid is cooled rapidly, it forms a glass, an amorphous phase of matter that is the epitome of disorder [2–6]. Nearly all [7] liquids have a larger entropy than crystalline solids but lose entropy much faster as temperature is decreased [8–10]. In 1948, Kauzmann recognized that there must exist a temperature at which the entropy of the liquid will cross the entropy of the crystal, but dismissed as paradoxical the possibility of such an “ideal glass” [8]. How could there be a liquid state that is both amorphous and highly ordered [9,11,12]? Here, we show a nonequilibrium mechanism for creating a two-dimensional zero configurational entropy jammed packing of polydisperse disks at zero temperature, which we term an ideal jammed packing. Such a packing represents the zero temperature limit of an ideal thermal glass, which is unreachable by physical processes due to a divergence in relaxation time [11,13]. This mechanism exploits transient degrees of freedom [14–25] and leads to zero configurational entropy at jamming, which is equivalent to our proposed definition of an ideal jammed packing as (1) having a fully triangulated contact network, (2) lacking long-range crystalline orientational and translational order, (3) being mechanically ultrastable, (4) being hyperuniform, and (5) having an anomalously high melting temperature equal to the Kauzmann temperature and an anomalously low melting density. We demonstrate that this ideal state

has all of the mechanical and thermal properties of a crystal while being entirely devoid of crystalline order. This Letter not only resolves the Kauzmann paradox but also demonstrates the existence of a thermodynamic glass phase for this two-dimensional model glass forming system. The creation of such an ideal glass or packing makes possible a complete exploration and explanation of two-dimensional jammed and glassy systems.

Packing protocols—A system of N disks in two dimensions has $2N$ translational degrees of freedom. At jamming, the system is isostatic, which means that every degree of freedom is constrained, and thus, the system must have $2N$ contacts between disks [26,27]. Since every contact is shared by two disks, each disk must then have an average coordination number of 4. A triangulated packing, by contrast, must have an average coordination number of 6, and thus, be maximally hyperstatic [28]. We achieve this by adding an additional degree of freedom to every disk in the form of a mutable radius.

The following protocol employs radii degrees of freedom to construct fully coordinated ideal amorphous packings in two dimensions while approximately preserving an input distribution of radii. This protocol builds on the use of transient degrees of freedom [21] and conformal circle packing [28].

Triangulated packings— N disks are placed randomly into a square simulation box with side length 1 and periodic

boundary conditions. Disks are assigned radii drawn from a log-normal distribution with 20% polydispersity [17], chosen to avoid crystallization [29]. Radii are scaled to an initial packing fraction $\varphi = 0.915$, chosen to result in highly coordinated (i.e., hyperstatic) packings [2,30]. The chosen value of φ leads to highly overjammed packings, which may be produced more quickly than critically jammed packings and are, thus, computationally convenient. Unjammed or critically jammed packings may also be used, producing qualitatively similar results. Particles interact through the soft sphere harmonic interaction potential,

$$U \equiv \sum_{\langle ij \rangle} \frac{1}{2} \left(1 - \frac{r_{ij}}{\sigma_{ij}} \right)^2 \Theta \left(1 - \frac{r_{ij}}{\sigma_{ij}} \right), \quad (1)$$

where the sum is over pairs of indices $\langle ij \rangle$, σ_{ij} is the sum of the i th and j th radii, and r_{ij} is the distance between centers. We use PyCudaPacking [31,32], a GPU based software package with an implementation of the FIRE algorithm [33], to adjust the positions and radii of the disks to find the inherent state structure, a local minimum of energy. Similarly to Hagh *et al.* [21], the radii degrees of freedom are subject to constraints on moments of the radius distribution in order to avoid falling into various trivial global minima. The result of such a minimization is nearly triangulated; however, these additional constraints necessarily introduce at least an equal number of “defects” into our system in the form of missing contacts.

In order to produce fully triangulated packings, we compute the radical Delaunay triangulation for the radii-minimized configurations. To find a fully triangulated hard sphere packing, we define a constraint for each edge in the radical Delaunay network requiring the distance between the centerpoints of contacting particles to be equal to the sum of their radii:

$$g_{\langle ij \rangle} \equiv \sum_{\alpha=1}^2 \left(x_j^\alpha - x_i^\alpha + \sum_{\beta=1}^2 \Lambda_{\beta}^\alpha z_{ij}^\beta \right)^2 - (r_i + r_j)^2 \quad (2)$$

where x_i^α is the position of particle i in dimension α , r_i is the radius of particle i , Λ is the lattice vector matrix, and z_{ij}^β is the β th component of the vector of integer lattice coordinates indicating which periodic image of particle i will be closest to the central image of particle j . Because the triangulated network is a maximal planar graph, the circle packing theorem guarantees the existence of a unique configuration that satisfies these constraints [28]. We write all of the degrees of freedom for our system as a single vector, \vec{c} , and place an artificial springlike attraction to the radii minimized system, \vec{c}_0 , to get the following Lagrangian:

$$\mathcal{L} \equiv |\vec{c} - \vec{c}_0|^2 + \sum_{\langle ij \rangle} \lambda_{\langle ij \rangle} g_{\langle ij \rangle} \quad (3)$$

where λ are the Lagrange multipliers. The total number of degrees of freedom in the system will be $2N$ (positions) + N (radii) + 4 (lattice vectors). However, from this we subtract the 2 (bulk traslations) + 1 (bulk rotation) + 1 (overall scale). This leaves us with $3N$ degrees of freedom and $3N$ constraints for a triangulated graph. This method produces critically jammed packings with no gaps between contacting particles and overlaps that are $\mathcal{O}(10^{-30})$. One may alternatively employ CirclePack [28] to produce a new disk packing from the radical Delaunay triangulation, if this level of precision is not required.

Our protocols yield packings at jamming fraction $\varphi \approx 0.910$, the densest such 2D amorphous packings of which we are aware. This density is meaningfully larger than that of the size-segregated hexagonal lattice of disks, $\varphi_{\text{hex}} = \pi/\sqrt{12} \approx 0.9069$, and much larger than the typical jamming density for conventionally prepared packings with the same disk size distributions as the triangulated packings, $\varphi_J \approx 0.849$ [2,30].

These processes leave the radii distribution approximately fixed relative to the radii minimized packings. We characterize this change in greater detail in the End Matter. We subsequently produce packings at a range of pressures by increasing the packing fraction as guided by the protocol described in [31].

From each triangulated packing, we produce conventionally jammed position-minimized packings with identical radii distributions by first randomizing positions and then minimizing energy with respect to position degrees of freedom only [34]. Conventionally jammed packings are illustrated in Fig. 1(b).

Properties of an ideal packing—We demonstrate that our triangulated packings meet all of the requirements for an ideal jammed packing.

(1) Ideal packings must be triangulated. The circle packing theorem provides a mechanism to convert any embeddable 2D graph into a disk packing with contact network equal to that graph. Generically, there will be a very large number of disk packings that share the same contact graph, and thus, the configurational entropy of a packing is bounded by that of the associated contact graph. However, for triangulated graphs there is a one-to-one mapping (unique up to trivial symmetries like rotations and mirrorings) between triangulated disk packings and triangulated graphs, and thus, the configurational entropy of the triangulated packing is equal to that of the underlying contact graph. As we show in the Supplemental Material [35], the specific configurational entropy of a triangulated graph goes to *zero* in the thermodynamic limit, and thus, the specific configurational entropy of triangulated packings also must go to zero [37–39]. Finally, a non-triangulated packing will necessarily and generically have neighboring particles that are separated by small gaps. Relaxing those gaps away must then lead to a denser packing. This will be impossible for a triangulated packing,

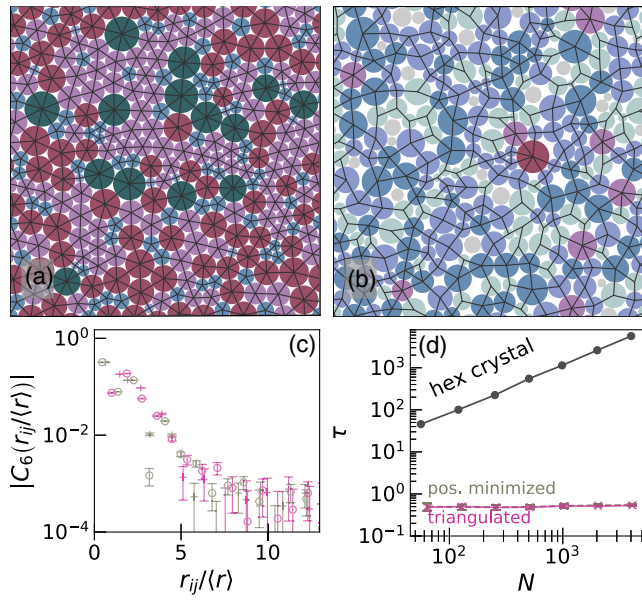


FIG. 1. (a) Triangulated packing and (b) conventionally jammed packing with $N = 256$ and an identical set of radii. The contact network is overlaid in black, while face coloring of disks corresponds to the number of contacts contacting neighbors (gray for zero, light green for three, periwinkle for four, blue for five, purple for six, red for seven, and teal for eight). (c) The orientational correlation function, C_6 , for triangulated packings (magenta) and conventionally jammed packings (tan) of $N = 2048$ (+'s) and 4096 (o's). (d) The finite size scaling for the translational order parameter, τ , for triangulated packings (magenta), conventionally jammed packings (tan), and the hexagonal crystal (black).

which must then be the densest packing possible with a given set of radii. By construction, the packings in this Letter have a fully triangulated contact network at the point of jamming.

(2) Ideal amorphous packings must, by definition, have no crystalline orientational or translational order. We demonstrate this lack in triangulated packings by computing the correlation function of the orientational order parameter ψ_6 [40] and the finite size scaling of the translational order metric τ [41].

The local orientational order parameter, $\psi_{6,i}$, is defined for disk i as

$$\psi_{6,i} \equiv \frac{1}{N_i} \sum_{j=1}^{N_i} e^{6i\theta_{ij}}, \quad (4)$$

where N_i is the number of neighbors, and θ_{ij} is the polar angle of the vector between particle i and neighbor j [40]. The correlation function $C_6(r)$

$$C_6(r) \equiv \langle \psi_6(\vec{r}_1) \psi_6^*(\vec{r}_2) \rangle_{|\vec{r}_2 - \vec{r}_1| = r}, \quad (5)$$

an average over ψ_6 pairs separated by distance r , is constant for a crystal but decays exponentially for both

the conventionally jammed and triangulated amorphous systems, as shown in Fig. 1(c). Note that C_6 for a crystal is always 1, irrespective of distance.

The translational order metric τ [41] is defined in 2D space as

$$\tau \equiv \frac{1}{D^2} \int [g(r) - 1]^2 d\vec{r}, \quad (6)$$

where $g(r)$ is the pair correlation function and D is a length scale chosen to be the average particle radius. Finite size scaling in τ indicates the degree of long-range translational order in a system. Poisson distributed points have $\tau = 0$ for all system sizes, amorphous disk packings maintain a constant nonzero value of τ with increasing N , and ordered systems show power law growth in τ with N . Figure 1(d) shows τ as a function of system size for the hexagonal crystal (circles), conventionally jammed systems (tan, labeled), and triangulated packings (violet, labeled).

Taken together, these two measurements demonstrate that triangulated packings are equally amorphous as conventionally jammed packings. Note that the absence of crystalline order does not preclude other forms of amorphous order, such as those revealed by point-to-set correlations, steric correlations [42], and other many-body correlation functions.

(3) Ideal packings must be mechanically ultrastable as a result of being the deepest well in the energy landscape. Ideal jammed packings must be strictly jammed, in the sense that no collective motions or strains lead to unjamming motions [43,44]. By employing a linear programming algorithm [43,44] that takes into consideration the one-sided contact potential, we find that all triangulated packings tested up to $N = 4096$ are strictly jammed just as crystalline systems are strictly jammed.

Figure 2 shows the mechanical properties of conventional packings, triangulated packings, and the hexagonal crystal. We calculate elastic moduli [45] and the vibrational density of states using the linear dynamical matrix of a packing. Triangulated packings are mechanically ultrastable as indicated by constant, and anomalously large, bulk and shear moduli as pressure is brought to zero, in contrast to the vanishing shear modulus at zero pressure found in conventionally jammed packings. Further, they play host to vibrational modes at vanishing pressure, which are governed by the Debye, or phononic [11,46], scaling of crystals and ultrastable systems and lack the Boson peak [47,48] of conventionally jammed packings. Just as in a 2D crystal, there is no phonon gap in the ideal packing because there is only a single “phase” throughout the entire system. Further, because the ideal packing is amorphous, there are no special lattice directions, and thus, the system is fully isotropic. In sum, the mechanical properties of triangulated packings are much more similar to those of crystals than to those of conventionally jammed packings [49], rendering them maximally distant from the point of marginality.

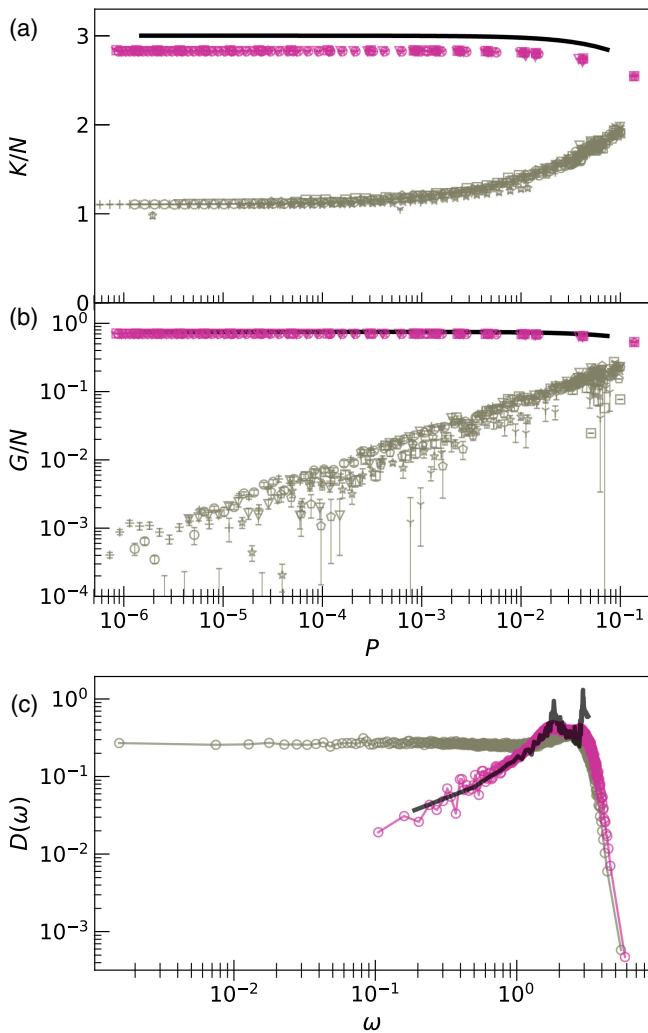


FIG. 2. (a) Bulk modulus per particle K/N is plotted as a function of pressure, P for triangulated packings (magenta points), conventionally jammed packings (tan points), and hexagonal crystals (black line) for N ranging from 64 to 4096 in powers of 2 (indicated by Y's, squares, pentagons, triangles, stars, +'s, o's, and hexagons, respectively). Moduli are averaged over 10 independent packing. Error bars indicate standard error. (b) Shear modulus per particle, G/N , is presented with the same colors and symbols. (c) Density of vibrational states, $D(\omega)$, is presented with the same colors and symbols; only $N = 4096$ is shown for clarity.

(4) An ideal packing must have vanishing long-range density fluctuations and thus be hyperuniform [50]. If it had such fluctuations, then one could cut out the lower density regions and replace them with copies of the higher density regions in order to achieve a denser packing. Further, low entropy is a necessary condition for hyperuniformity, which is possible only for states of zero complexity [51].

We show that our triangulated packings are hyperuniform by directly measuring the long wavelength (and thus, the small wave number, \vec{k}) scaling in the spectral density [52],

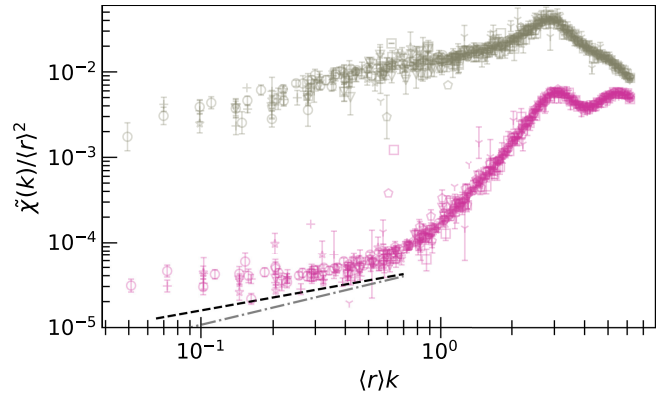


FIG. 3. Binned averages of spectral density $\tilde{\chi}$, scaled by $\langle r \rangle$ to collapse curves from $N = 64$ –8192; respective markers are, in increasing powers of 2, Y's, squares, pentagons, triangles, stars, +'s, o's, and hexagons. Color indicates protocol; tan for position-minimized packings and magenta for triangulated packings. Dashed lines with slope of 1/2 (black) and 2/3 [43] (gray) are overlaid as a visual guide. Error bars indicate standard geometric error of mean for each point; points without error bars are unaveraged.

$$\tilde{\chi}(\vec{k}) \equiv \frac{|\sum_{j=1}^N \exp(-i\vec{k} \cdot \vec{x}_j) \tilde{m}(\vec{k}; R_j)|^2}{V}, \quad (7)$$

where $V = 1$ is the box volume,

$$\tilde{m}(\vec{k}; R_j) \equiv \frac{2\pi R_j}{|\vec{k}|} J_1(R_j|\vec{k}|), \quad (8)$$

and J_1 is the Bessel function of the first kind with order 1. We take a Fourier space angular average to produce $\tilde{\chi}(k)$, shown in Fig. 3. Hyperuniformity corresponds to a vanishing value of $\tilde{\chi}(k)$ in the limit of small $k \equiv |\vec{k}|$ [50,52]. While both conventionally jammed and triangulated packings show approximately power law behavior for small k [53–56], the triangulated packings show a far greater degree of effective hyperuniformity [57].

(5) The melting temperature (for soft spheres) and the melting density (for hard spheres) measure the thermodynamic stability of a glass and encode information about the height of the barriers about the stable basin. In an ideal glass, the melting temperature should be higher and the melting density should be lower than that of any other glass. Using standard Monte Carlo techniques, we measure the relaxation time of the thermal packing seeded by the positions of the jammed state at various temperatures (soft spheres) or deflated densities (hard spheres) to identify the point at which the relaxation time diverges. We identify this point as the melting point of each packing (see End Matter for details).

We find that the conventional packings have $T_m < 10^{-4}$ for soft spheres and $\varphi_m = 0.824(5)$ for hard spheres, while

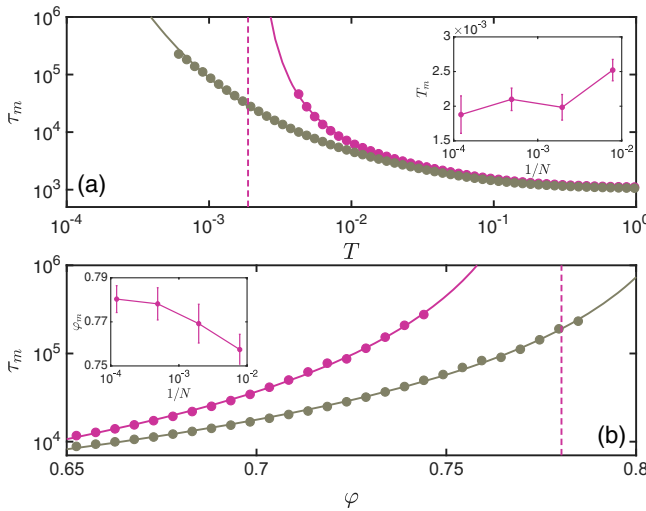


FIG. 4. Measurements of the relaxation time for a sample triangulated packing (magenta) and conventionally jammed packing (tan), each with $N = 8192$ using 10 thermal averages for (a) thermal soft spheres and (b) hard spheres. Solid line fits are to the modified VFT form of Eq. (B1) and to the power-law diffusion form of Eq. (B2), respectively, and dashed lines show the ideal glass melting point. Insets show a lack of statistically significant finite size scaling for $N > 128$.

the triangulated packings have a melting temperature of $T_m = 0.00189(10)$ for soft spheres and $\varphi_m = 0.780(6)$ for hard spheres. The uncertainty here indicates a 95% confidence interval, and no statistically significant finite size effects are seen for $N > 128$.

These results stand in opposition to previous work done on ultrastable (but not ideal) 2D hard sphere glasses, which can be read to suggest $T_m = 0$ for finite size systems [49,58]. This distinction is likely due to the difference between truly ideal systems and those that are merely ultrastable.

Of course, the Mermin-Wagner-Hohenberg (MWH) theorem [59,60] would seemingly require that the melting temperature in 2D should converge to zero in the thermodynamic limit. We see no evidence of such convergence. MWH assumes continuous symmetries for which the length scale diverges. This is why MWH is seemingly violated in, for example, the Kosterlitz-Thouless-Halperin-Nelson-Young two dimensional crystalline melting scenario [61], where this scale is extremely large, yet finite. Further, recent work has questioned the applicability of MWH to amorphous phase transitions [62–64].

Conclusion—The nature of the glass transition remains a mystery, and the question of whether an ideal configuration exists lies at the heart of this mystery [9]. The constructive scheme presented herein demonstrates not only that ideal packings exist but that they have superlative structural, mechanical, and thermal properties. This represents a leap forward in understanding the complex energy landscapes underlying disordered systems and places the existence of a

thermodynamic glass phase on firm footing. By working backward from the ideal system through the introduction of defects, we hope to fully explore the glassy landscape of two-dimensional amorphous systems. Ideal packings are also interesting from a practical perspective. Such packings are fully amorphous while presenting the bulk material and thermal properties of crystalline materials: ultrastability, hyperuniformity, and high melting temperatures, all properties that are desirable from an industrial perspective. However, novel approaches will be necessary to create such packings in practice, as they are not accessible through common thermal or mechanical processes. To create such systems in practice, a physical implementation of our algorithm would have to be developed.

Acknowledgments—We thank Francesco Arceri, Ludovic Berthier, Varda Hagh, Sascha Hilgenfeldt, and Ken Stephenson for valuable discussions. This work benefited from access to the University of Oregon high performance computer, Talapas. This work was supported by the Simons Foundation No. 454939 (V. B. L., R. C. D., and E. I. C.).

Data availability—The data that support the findings of this article are openly available at [65]. CirclePack is available at [66].

- [1] M. Planck, *Vorlesungen über Thermodynamik* (De Gruyter, Leipzig, 1905).
- [2] C. S. O’Hern, L. E. Silbert, A. J. Liu, and S. R. Nagel, *Phys. Rev. E* **68**, 011306 (2003).
- [3] D. Turnbull, *Contemp. Phys.* **10**, 473 (1969).
- [4] M. D. Ediger, C. A. Angell, and S. R. Nagel, *J. Phys. Chem.* **100**, 13200 (1996).
- [5] P. G. Debenedetti and F. H. Stillinger, *Nature (London)* **410**, 259 (2001).
- [6] P. Charbonneau, J. Kurchan, G. Parisi, P. Urbani, and F. Zamponi, *Annu. Rev. Condens. Matter Phys.* **8**, 265 (2017).
- [7] F. Smalldenburg and F. Sciortino, *Nat. Phys.* **9**, 554 (2013).
- [8] W. Kauzmann, *Chem. Rev.* **43**, 219 (1948).
- [9] L. Berthier and G. Biroli, *Rev. Mod. Phys.* **83**, 587 (2011).
- [10] P. Charbonneau, Y. Jin, G. Parisi, and F. Zamponi, *Proc. Natl. Acad. Sci. U.S.A.* **111**, 15025 (2014).
- [11] C. P. Royall, F. Turci, S. Tatsumi, J. Russo, and J. Robinson, *J. Phys. Condens. Matter* **30**, 363001 (2018).
- [12] A. Cavagna, *Phys. Rep.* **476**, 51 (2009).
- [13] L. Berthier, P. Charbonneau, D. Coslovich, A. Ninarello, M. Ozawa, and S. Yaida, *Proc. Natl. Acad. Sci. U.S.A.* **114**, 11356 (2017).
- [14] D. Gazzillo and G. Pastore, *Chem. Phys. Lett.* **159**, 388 (1989).
- [15] M. D. Ediger, *J. Chem. Phys.* **147**, 210901 (2017).
- [16] H. Ikeda, F. Zamponi, and A. Ikeda, *J. Chem. Phys.* **147**, 234506 (2017).
- [17] A. Ninarello, L. Berthier, and D. Coslovich, *Phys. Rev. X* **7**, 021039 (2017).
- [18] G. Szamel, *Phys. Rev. E* **98**, 050601(R) (2018).

[19] C. Rodriguez-Tinoco, M. Gonzalez-Silveira, M. A. Ramos, and J. Rodriguez-Viejo, *Riv. Nuovo Cimento* **45**, 325 (2022).

[20] S. Kim and S. Hilgenfeldt, *Phys. Rev. Lett.* **129**, 168001 (2022).

[21] V. F. Hagh, S. R. Nagel, A. J. Liu, M. L. Manning, and E. I. Corwin, *Proc. Natl. Acad. Sci. U.S.A.* **119**, e2117622119 (2022).

[22] S. Kim and S. Hilgenfeldt, [arXiv:2402.08390](https://arxiv.org/abs/2402.08390).

[23] G. Kapteijns, W. Ji, C. Brito, M. Wyart, and E. Lerner, *Phys. Rev. E* **99**, 012106 (2019).

[24] C. Brito, E. Lerner, and M. Wyart, *Phys. Rev. X* **8**, 031050 (2018).

[25] Y. Wang, Z. Qian, H. Tong, and H. Tanaka, *Nat. Commun.* **16**, 1398 (2025).

[26] J. C. Maxwell, *Philos. Mag.* **27**, 294 (1864).

[27] V. F. Hagh and M. F. Thorpe, *Phys. Rev. B* **98**, 100101(R) (2018).

[28] K. Stephenson, *Introduction to Circle Packing: The Theory of Discrete Analytic Functions* (Cambridge University Press, New York, 2005).

[29] H. Tong, P. Tan, and N. Xu, *Sci. Rep.* **5**, 15378 (2015).

[30] C. S. O'Hern, S. A. Langer, A. J. Liu, and S. R. Nagel, *Phys. Rev. Lett.* **88**, 075507 (2002).

[31] P. Charbonneau, E. I. Corwin, G. Parisi, and F. Zamponi, *Phys. Rev. Lett.* **114**, 125504 (2015).

[32] P. K. Morse and E. I. Corwin, *Phys. Rev. Lett.* **112**, 115701 (2014).

[33] E. Bitzek, P. Koskinen, F. Gähler, M. Moseler, and P. Gumbsch, *Phys. Rev. Lett.* **97**, 170201 (2006).

[34] P. Charbonneau, E. I. Corwin, G. Parisi, and F. Zamponi, *Phys. Rev. Lett.* **109**, 205501 (2012).

[35] See Supplemental Material at <http://link.aps.org/supplemental/10.1103/vldy-r77w>, which includes Ref. [36].

[36] M. C. Holmes-Cerfon, *SIAM Rev.* **58**, 229 (2016).

[37] E. A. Bender, Z. Gao, and N. C. Wormald, *Electron. J. Comb.* **9**, R43 (2002).

[38] O. Giménez and M. Noy, *J. Am. Math. Soc.* **22**, 309 (2009).

[39] G. Chapuy, E. Fusy, O. Giménez, B. Mohar, and M. Noy, *J. Comb. Theory Ser. A* **118**, 748 (2011).

[40] B. I. Halperin and D. R. Nelson, *Phys. Rev. Lett.* **41**, 121 (1978).

[41] S. Torquato, G. Zhang, and F. H. Stillinger, *Phys. Rev. X* **5**, 021020 (2015).

[42] X. Fan, D. Xu, J. Zhang, H. Hu, P. Tan, N. Xu, H. Tanaka, and H. Tong, [arXiv:2404.17675](https://arxiv.org/abs/2404.17675).

[43] A. Donev, S. Torquato, F. H. Stillinger, and R. Connelly, *J. Comput. Phys.* **197**, 139 (2004).

[44] A. Donev, S. Torquato, F. H. Stillinger, and R. Connelly, *J. Appl. Phys.* **95**, 989 (2004).

[45] R. C. Dennis and E. I. Corwin, *Phys. Rev. Lett.* **128**, 018002 (2022).

[46] D. Xu, S. Zhang, H. Tong, L. Wang, and N. Xu, *Nat. Commun.* **15**, 1424 (2024).

[47] M. L. Manning and A. J. Liu, *Europhys. Lett.* **109**, 36002 (2015).

[48] P. Charbonneau, E. I. Corwin, G. Parisi, A. Poncet, and F. Zamponi, *Phys. Rev. Lett.* **117**, 045503 (2016).

[49] L. Berthier, P. Charbonneau, A. Ninarello, M. Ozawa, and S. Yaida, *Nat. Commun.* **10**, 1508 (2019).

[50] S. Torquato and F. H. Stillinger, *Phys. Rev. E* **68**, 041113 (2003).

[51] M. J. Godfrey and M. A. Moore, *Phys. Rev. Lett.* **121**, 075503 (2018).

[52] C. E. Zachary, Y. Jiao, and S. Torquato, *Phys. Rev. Lett.* **106**, 178001 (2011).

[53] M. Skoge, A. Donev, F. H. Stillinger, and S. Torquato, *Phys. Rev. E* **74**, 041127 (2006).

[54] E. Tjhung and L. Berthier, *Phys. Rev. Lett.* **114**, 148301 (2015).

[55] D. Hexner and D. Levine, *Phys. Rev. Lett.* **114**, 110602 (2015).

[56] A. Ikeda, L. Berthier, and G. Parisi, *Phys. Rev. E* **95**, 052125 (2017).

[57] S. Torquato, *Phys. Rep.* **745**, 1 (2018).

[58] L. Santen and W. Krauth, *Nature (London)* **405**, 550 (2000).

[59] P. C. Hohenberg, *Phys. Rev.* **158**, 383 (1967).

[60] N. D. Mermin and H. Wagner, *Phys. Rev. Lett.* **17**, 1133 (1966).

[61] P. Sampedro Ruiz, Q.-l. Lei, and R. Ni, *Commun. Phys.* **2**, 70 (2019).

[62] S. Vivek, C. P. Kelleher, P. M. Chaikin, and E. R. Weeks, *Proc. Natl. Acad. Sci. U.S.A.* **114**, 1850 (2017).

[63] H. Shiba, Y. Yamada, T. Kawasaki, and K. Kim, *Phys. Rev. Lett.* **117**, 245701 (2016).

[64] B. Illing, S. Fritschi, H. Kaiser, C. L. Klix, G. Maret, and P. Keim, *Proc. Natl. Acad. Sci. U.S.A.* **114**, 1856 (2017).

[65] V. Bolton-Lum, R. Cameron Dennis, P. Morse, E. Corwin, Two Dimensional Ideal Packing Repository [Dataset] (2025), [10.5061/dryad.fqz612k5s](https://doi.org/10.5061/dryad.fqz612k5s).

[66] www.circlepack.com.

[67] D. Frenkel and B. Smit, *Understanding Molecular Simulation: From Algorithms to Applications*, 2nd ed., Computational Science Series Vol. 1 (Academic Press, San Diego, 2002).

[68] P. Charbonneau, Y. Hu, J. Kundu, and P. K. Morse, *J. Chem. Phys.* **156**, 134502 (2022).

[69] L. S. Garcia-Colin, L. F. del Castillo, and P. Goldstein, *Phys. Rev. B* **40**, 7040 (1989).

[70] F. Arceri, F. P. Landes, L. Berthier, and G. Biroli, in *Statistical and Nonlinear Physics*, edited by B. Chakraborty, Encyclopedia of Complexity and Systems Science Series (Springer US, New York, 2022), pp. 229–296.

[71] F. Ritort and P. Sollich, *Adv. Phys.* **52**, 219 (2003).

[72] J. Kurchan, G. Parisi, P. Urbani, and F. Zamponi, *J. Phys. Chem. B* **117**, 12979 (2013).

End Matter

Diameter distribution—Figure 5 shows that triangulated packings with initial radii drawn from a 20% polydispersity log-normal distribution are distributed more closely to a 26% polydisperse log-normal distribution

after radii minimization. The final step of creating the perfectly triangulated packing (illustrated in Figure 1) typically involves changes to particles' relative radii on the order of 0.2%. Note that radius minimized packings

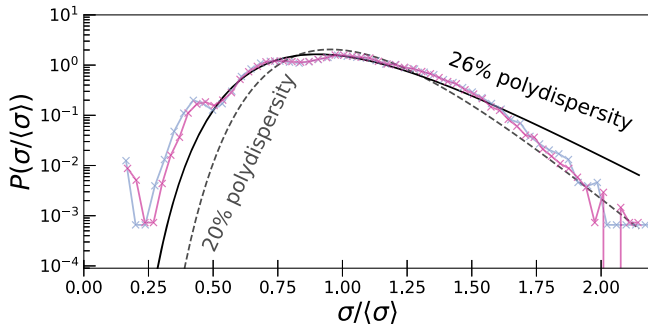


FIG. 5. The probability distribution of disk diameters, $P(\sigma)/\langle\sigma\rangle$, averaged over 10 packings of 4096 disks. The starting distribution is at 20% polydispersity (gray dashed line), the distribution after radii minimization is plotted as gray x's, the distribution after triangulation is plotted as magenta triangles, and for comparison, a 26% polydispersity distribution is shown in black.

are already quite close to a fully triangulated state, and thus, require only minimal changes in radii.

Measuring the melting point—To measure the melting temperature, we apply simple constant volume Monte Carlo dynamics at a range of temperatures T using standard Metropolis sampling with the Boltzmann weight $\exp(-\Delta U/T)$ [67] using the same packing fraction ϕ for both the conventional jammed packings and the triangulated packings. For each temperature, we measure the time τ_m that it takes for the system to forget its initial state (i.e., the state-overlap parameter becomes $1/e$) [68]. The melting temperature T_m is then extracted from a fit to a modified Vogel-Fulcher-Tammann (VFT) form [69],

$$\tau_m \equiv \tau_0 \exp \left[\left(\frac{DT_m}{T - T_m} \right)^c \right], \quad (B1)$$

where D is a dimensionless material dependent constant. The standard VFT equation with $c = 1$ fits our data poorly, in large part due to the large polydispersity, which generically leads to a wide variety of minima, and thus dynamical heterogeneities. We thus take inspiration

from other models with a high degree of dynamical heterogeneity that suggest a stretched exponential form in the viscosity and relaxation times [70,71], and thus, a variable c . This exponent then relates to the ductility of the glass, with higher values of c indicating stronger glasses [5].

Figure 4 shows that the conventional packings have $T_m < 10^{-4}$, while the triangulated packings have a melting temperature at least an order of magnitude larger, $T_m = 0.00189(10)$, with the error bar indicating a 95% confidence interval. Here, the melting temperature remains constant and nonzero to within the reported fitting error for system sizes $N > 128$, indicating a lack of finite-size scaling. The presence of a truly nonzero melting temperature in a 2D system suggests a violation of the Mermin-Wagner-Hohenberg theorem, which forbids spontaneous symmetry breaking. There are at least two caveats to consider: (1) it is possible that an amorphous glass breaks the continuous symmetry of the liquid, and thus, does not require a violation of MWH [62–64]; and (2) the KTHNY scenario [61] offers the possibility of a transition between quasi-long-ranged and long-ranged ordering, which also would not violate MWH.

The process of determining the melting density follows a similar routine by using constant volume Monte Carlo dynamics at different packing fractions φ with hard sphere Metropolis sampling starting from the seeded ideal (or nonideal) glass positions. Here, however, the relaxation follows a simple power law scaling,

$$\tau_m = D(\varphi_m - \varphi)^{-\gamma}, \quad (B2)$$

where for the ideal glass at $N = 8192$, we find $D = 57(12)$, $\varphi_m = 0.780(6)$, and $\gamma = 2.6(3)$, and for the nonideal glass, we find $D = 150(30)$, $\varphi_m = 0.824(5)$, and $\gamma = 2.28(15)$. Curiously, we find that this seeded diffusion process has a critical exponent γ , which is consistent with the mean-field glass value of $\gamma = 2.33786$ [72] unlike the monodisperse counterparts [68], which undershoot this value. As with the melting temperature, we observe no statistically significant finite size scaling for $N > 128$, indicating that the thermodynamic melting density is $\varphi_m = 0.780(6)$.